AMERICAN SCIENTIFIC PUBLISHERS

Energy and Environment Focus
Vol. 2, pp. 1–8, 2014
(www.aspbs.com/efocus)

ARTICLE

Using Thin Films of Rutile-Phase TiO_2 Nanoparticles as Photoactive Material in Metal-Semiconductor Structures with Low Thermal Processing

Joel Molina[1,*], Carlos Zuniga[1], Eunice Mendoza[2], Jose-Luis Sanchez-Salas[2], Edmundo Gutierrez[1], and Erick R. Bandala[2]

[1]*Optics and Electronics (INAOE) Electronics Department, National Institute of Astrophysics, Luis Enrique Erro #1, Sta. Maria Tonantzintla 72840, Puebla. Mexico*
[2]*Universidad de las Americas, Puebla (UDLAP) Grupo de Investigacion en Energia y Ambiente. Sta. Catarina Martir, Cholula 82710 Puebla, Mexico*

ABSTRACT

Rutile-phase TiO_2 nanoparticles are embedded within an organic SiO_2 matrix (Spin-On Glass) and the final suspension is deposited by spinning on (a) thin aluminum stripes or (b) in between thin aluminum films and ultra-thin titanium stripes. The maximum processing temperature for both devices is 220 °C. The first device is a "horizontal" TiO_2:SiO_2/Al/Glass photoactive structure which is then electrically characterized under dark and illuminated conditions (*I*–*V*-Light) so that the total resistance of a simple aluminum stripe is measured before/after ultraviolet-visible (UV-Vis) irradiation. Compared to dark conditions, excess carriers are photogenerated within the TiO_2 nanoparticles during light exposure and they are transferred to both ends of the aluminum stripe after applying a low potential difference. A large decrease in the resistance of the aluminum stripe (down to 43% of its original value) is obtained when this horizontal structure is irradiated with UV-B light thus acting as a *photoresistor*. The second device is a "vertical" Ti/TiO_2:SiO_2/Al/Glass photoactive structure. Here, the path for photogenerated and electrically-driven carriers occurs vertically, or inside a Metal-Insulator-Metal (MIM) capacitor. Because of the ultra-thin titanium layer (100 Å in thickness), this gate electrode is highly transparent to most of the UV-Vis irradiation so that when all carriers are being photogenerated, they are almost immediately separated at the top/bottom electrodes by a small applied electric field due to the thin and high-dielectric constant of the photoactive TiO_2:SiO_2 film. This way, a fast and large increase/decrease in gate current (about 4–7 orders of magnitude) is observed when this device is under illumination/dark conditions. This vertical structure operates as a *photocapacitor*, where all photogenerated carriers could be efficiently stored within the MIM capacitor itself and thus, enable simultaneous conversion and storage of solar energy in the same device.

KEYWORDS: Low Temperature Processing, Rutile TiO_2, TiO_2 Nanoparticles, Photoresistor, Photocapacitor, Solar Cell.

1. INTRODUCTION

It is widely known that TiO_2 (whether in *rutile*, *anatase* or *brookite* crystalline phases) posses enough photocatalytic properties than can be used for efficient conversion of solar energy into electric current if proper device architectures are provided. Photogeneration of electron–hole pairs in TiO_2 occurs naturally when this material is irradiated under high energy conditions like ultraviolet-visible (UV-Vis) light sources, and whose energy (in electron-Volts, eV) is well matched to the energy gap (E_g) of TiO_2. After electron–hole photogeneration, an efficient mechanism for separation of these carriers is needed and the simplest way to achieve this is by developing a large enough electric field so that the negative and positive charges are attracted to the positive and negative polarities of the applied voltage respectively. These very simple mechanisms of photogeneration and carrier separation by electric field are what most solar cells (mostly based in *P*–*N* junctions) use for

*Author to whom correspondence should be addressed.
Email: jmolina@inaoep.mx
Received: 2 October 2013
Accepted: 8 November 2013

conversion and handling of an electric current whose magnitude is in direct proportion to the energy and density of radiation being absorbed.

On the other hand, the use of TiO_2 nanoparticles for energy conversion is quite attractive given its high contact surface area as compared to a dense bulk film of the same material. This is important since, after irradiation with the proper light sources, a larger density of photogenerated carriers are expected in devices using photoactive nanoparticles. These photogenerated carriers could then be used for more efficient energy conversion ad even, simultaneous energy conversion and storage of the carriers in the same device. In this sense, and even though rutile-phase TiO_2 is considered a very inefficient material in terms of its photocatalytic activity,[1,2] the use and development of this semiconductor material is quite important since the synthesis of TiO_2 usually produces a rutile phase quite easily, with relatively low concentration of impurities and also, economically. Additionally, the synthesis of anatase-phase TiO_2 is more complicated, usually involving complex chemistry and/or doping with some metal or non-metal elements in order to increase its photocatalytic activity when exposed to UV or visible irradiation.[3–6]

In this work, we embed rutile-phase TiO_2 nanoparticles (*np*-TiO_2) within an organic SiO_2 matrix and the final suspension is deposited on (a) thin aluminum stripes or (b) in between thin aluminum films and ultra-thin titanium stripes. These two structures are so-called "horizontal" and "vertical" metal-semiconductor structures and they operate as simple *photoresistor* and *photocapacitor* devices respectively. Both horizontal and vertical structures are then electrically characterized under dark and light conditions (*I*–*V*-Light) so that the total resistance of a simple aluminum stripe or the resistance state of a thin TiO_2:SiO_2 insulator are measured and correlated before and after light irradiation. For the horizontal TiO_2:SiO_2/Al/Glass structure, the highest density of photogenerated carriers is obtained when the device is irradiated with UV-B light so that the total aluminum resistance is reduced by about 43%. For the vertical Ti/TiO_2:SiO_2/Al/Glass structure, a sudden and large increase/decrease in gate current (about 4–7 orders of magnitude) is obtained when the device is under illumination/dark conditions and is simultaneously biased with a small applied bias. Since this vertical device is a special MIM capacitor (with the top electrode made of titanium of only 100 Å in thickness), this last device has the potential to simultaneously convert and self-store must of the solar energy that is being absorbed by the TiO_2 nanoparticles within the oxide. This device then operates like a very simple *photocapacitor*.[7,8] The *state-of-the-art* regarding these latest structures makes use of complex layered structures going from photo-rechargeable textiles for wearable power supplies,[9] up to dye-sensitized solar cells (DSSC) connected in series with Li-ion batteries, metal oxides and/or TiO_2 nanotube arrays in order to increase energy conversion efficiency.[10–12] However, because of increasing fabrication complexity and use of a third additional electrode (in order to switch between the functions of energy conversion, storage and output) which consumes extra energy and increase cost of fabrication, a simpler two-electrode device is needed and that requirement is met by our proposed device structures.

Finally, it is also important to notice that in order to keep long enough photocarrier lifetimes before recombination (thus increasing quantum efficiency for proper light conversion into electric current), a low thermal processing of all materials involved is needed during fabrication of the devices. In both our horizontal and vertical devices, a low thermal budget has been kept by using a maximum processing temperature of 220 °C, which can be even lowered to 100 °C in order to evaporate mostly water and some organic solvents off the TiO_2:SiO_2 ~~suspensionand~~ for film densification. This low-thermal budget process makes these devices ideal for fabrication on large-area flexible substrates with the potential to decrease their final costs for widespread use.

2. EXPERIMENTAL DETAILS

2.1. Deposition of Thin Metal Films

For the horizontal TiO_2:SiO_2/Al/Glass structures, and previous to depositing TiO_2 nanoparticles on Corning glass slides (2947, size of 75 mm × 25 mm~~, from Corning~~), the initial substrates were degreased by ultrasonic cleaning in trichloroethylene and acetone (10 min and 10 min respectively). After cleaning ~~of~~ the glass slides, 400 nm of aluminum was deposited on one surface of the substrates by *e*-beam evaporation under ultra-high vacuum conditions (UHV). A metal mask was used during this metallization so that relatively large stripes of aluminum (18 mm × 3 mm) were left on the glass slides and these substrates are now ready for deposition of TiO_2:SiO_2 suspensions. For the vertical Ti/TiO_2:SiO_2/Al/Glass structures, 400 nm of aluminum are initially deposited on one surface of the cleaned glass slides without using any metal mask. This initial aluminum layer works as the bottom electrode of the MIM structure. After deposition of the TiO_2:SiO_2 suspension, 100 Å of titanium is then deposited by *e*-beam evaporation (also in UHV conditions). This second metallization with titanium is now performed through a metal mask so that stripes (same size as before) are left on top of the final vertical structure. For all aluminum and titanium metallization, a deposition rate of 1 Å/sec inside a vacuum of 10^{-7} Torr ~~were~~ used.

2.2. Preparation of Thin Films Based on Rutile-Phase TiO_2 Nanoparticles

A low-organic content or silicate-type spin-on glass (SOG)-based SiO_2 (700Bfrom Filmtronics, Corp.) was used ~~asa~~ matrix for immobilization of TiO_2 nanoparticles. The average diameter of these TiO_2 nanoparticles is 360 nm before synthesis (R-706 with 93% purity, as

stated by Dupont). Initially, specific amounts of commercial TiO_2 are suspended in deionized water by hydrolyzing this TiO_2:H_2O mixture in a water bath (45 °C, with variation of ±2 °C, 30 min) and then SOG-based SiO_2 was added. The final TiO_2:SiO_2:H_2O mixture was again heated in a water bath (80 °C, 1 hr) in order to obtain a stable and homogeneous TiO_2 suspension (minimizing nanoparticles' aggregation and/or sedimentation). The concentration ratios of TiO_2 to SiO_2:H_2O were 200, 100, 50 and 10 $mg \cdot mL^{-1}$ and these suspensions were labeled as A, B, C and D respectively. Each concentration of TiO_2 nanoparticles was measured with an analytical balance AG285 from Mettler-Toledo. The final TiO_2:SiO_2:H_2O suspensions were directly applied on one surface of already metalized glass slides and sequentially spun first at 3000 rpm, 30 sec, and then 4000 rpm, 15 sec in order to obtain uniform thin layers of TiO_2 embedded in SiO_2. After spinning, all films ~~(A) (D)~~ were baked for 2 hours using a hot plate at 220 °C under N_2 flow (99.99% purity) in order to evaporate mostly water and some of the organic solvents present in the SOG-based SiO_2 matrix. For FTIR characterization, the same processing sequence was followed and the final suspension was applied on prime-grade *P*-type silicon wafers (100) with resistivity of 5–10 Ω · cm in order to eliminate most of the organic and impurity elements present within the Corning glass slides. For physical and chemical characterization, all A–D suspensions were directly deposited on clean glass slides or silicon wafers (without any metallization), whereas only the most concentrated suspension (A suspension) was used for

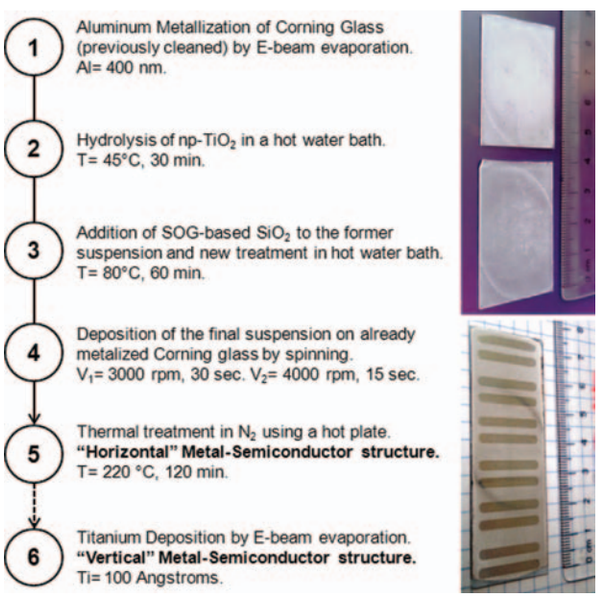

Fig. 1. Processing flow for fabrication of "*horizontal*" and "*vertical*" structures using TiO_2 nanoparticles as photoactive material. The photo at the top shows TiO_2 nanoparticles directly deposited on glass slides (without metallization) while the bottom picture shows a full vertical structure.

fabrication of the horizontal and vertical structures and therefore, for *I*–*V*-Light characterization. The process flow for fabrication of both horizontal and vertical structures is briefly summarized in Figure 1 ~~(along)~~ with a top picture of two Corning glasses covered with the resulting films (suspensions A and B only) and a bottom picture depicting the vertical structure (Ti/TiO_2:SiO_2/Al/Glass).

2.3. Chemical and Physical Characterization

Dynamic-light scattering measurements (DLS by Nanotrac Wave, from Microtrac) were done in order to determine the final size distribution of TiO_2 nanoparticles after the whole synthesis process. The profile of size distribution for TiO_2 nanoparticles is obtained with high accuracy by DLS (close to 100% signal intensity), thus giving a direct estimation of the homogeneity of the TiO_2 nanoparticles in the final suspension. Also, thicknesses for all films were measured by profilometry (DEKTAK, V200-SI) after partially etching the TiO_2/SiO_2 film using a strong acid solution composed of diluted HF (HF:H_2O, 1:2 volume ratio). The crystalline phases of the resulting TiO_2-based films were obtained after X-Ray Diffraction (XRD) measurements (Empyrean, from PANalytical), with a scanning step of 0.02°, using Cu–K_α radiation with $\lambda = 1.5406$ Å as an X-ray source. The band-gap energies E_g of the resulting films were calculated using optical transmittance data measured with an UV-Vis absorption spectrometer (LAMBDA 3B with double beam from Perkin Elmer, Inc., and using Corning glass as ~~substrate)and~~ the Tauc method.[13] Chemical compositional analyses for all films were obtained by FTIR spectrum measurements in absorbance mode with a Bruker Vector-22 system after 5 min of purge in N_2. The samples were measured against crystalline silicon substrate or SOG-based silicon ~~dioxideon~~ glass (both used as references).

2.4. Electrical Characterization Under Dark and Illumination Conditions (*I*–*V*-Light)

As stated before, only the most concentrated suspension (A suspension) was used for fabrication of the horizontal and vertical ~~structuresand~~ therefore, for *I*–*V*-Light characterization (*I*–*V* measurements under dark/illumination conditions). For characterizing these final structures we have used an HP4156B semiconductor parameter analyzer at 300 K. As light source, we used natural light conditions of sunlight coming indirectly to the laboratory room, sunlight plus a white lamp put right above all the structures and an UV-B lamp. For the horizontal structure, an *I*–*V* sweep was applied to the ends of the same aluminum stripe while limiting the current compliance to 100 mA. For the vertical structure, an *I*–*V* measurement in sampling mode was used where the gate current was constantly monitored with time while the gate voltage was kept constant at $V_g =$ 10 V. In this latter case, the gate current was limited to 100 μA.

ARTICLE

3. RESULTS AND DISCUSSION

3.1. Schematics and Physical Characteristics of TiO_2 and Metal-Semiconductor Structures

Figure 2 shows the schematics for the (a) horizontal TiO_2:SiO_2/Al/Glass planar structure (3-D and top view) and the (b) vertical Ti/TiO_2:SiO_2/Al/Glass MIM structure (3-D view). In both cases, and because of their fabrication method, we promote a uniform distribution of the TiO_2 nanoparticles within the oxide matrix so that these nanoparticles should have almost the same diameter size and separation in between as well. For the horizontal structure, the I–V-Light characterization takes place by measuring a current flow at both ends of the same bottom aluminum electrode while both bottom and top electrodes are used in the vertical structure. In the horizontal ~~structureand~~, by applying a small potential difference to the same bottom aluminum electrode, photogenerated carriers are then injected into this metal (and separated by the electric field) thus decreasing its original resistance. In the vertical structure, a potential difference applied to both bottom/top electrodes would separate all photogenerated carriers thus increasing the level of the original gate current (decreasing the original resistance state of the combined TiO_2:SiO_2). In both cases, we do not take into account most of the physical mechanisms responsible for lowering the quantum efficiency of the structures: trapping, recombination, phonon interaction, annihilation, interface defects, etc. However, those mechanisms and defects are important in order to properly engineer the fabrication process for these structures and then, increase their quantum efficiency for less energetic sources like visible irradiation (reducing E_g or increasing the photogenerated carrier lifetimes before recombination).

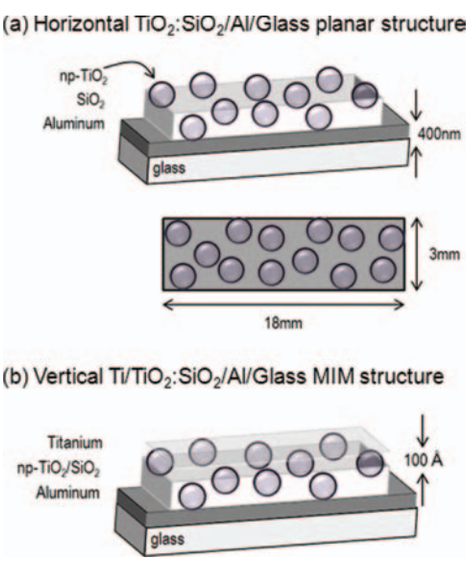

Fig. 2. Schematics showing the (a) horizontal TiO_2:SiO_2/Al/Glass planar structure (3-D and top view) and (b) vertical Ti/TiO_2:SiO_2/Al/Glass MIM structure (3-D view).

On the other hand, before deposition of TiO_2 nanoparticles by spinning, it is important to sonicate all the prepared suspensions since they do have a tendency to agglomerate/aggregate after dispersion and settling within the liquid suspension. The average physical size for sonicated TiO_2 nanoparticles is around 300 nm (close to the nominal diameter of 360 nm). After deposition and thermal treatment of the prepared suspensions, thicker TiO_2 films were obtained for more concentrated suspensions as expected. For samples A, B, C and D, the measured film thicknesses were 654, 533, 443 and 210 nm respectively.[14] Given that for sample D there is a minimum amount of TiO_2 nanoparticles (only 10 $mg \cdot mL^{-1}$), the final average thickness for this ~~filmwas~~ kept below the average nanoparticles' diameter because of the reduction in most of the SiO_2 thickness by enhanced H_2O dilution and also, because more water per volume induces further dilution or dispersion of previously agglomerated TiO_2 nanoparticles. From X-ray diffraction measurements,[14] samples A–B (with concentrations of 200 and 100 $mg \cdot mL^{-1}$ respectively) presented the sharpest diffraction peaks for rutile phase TiO_2 including the broad amorphous phase from both the SiO_2 matrix and the glass slide (used for TiO_2 immobilization and mechanical support purposes respectively). In particular, sample A showed the clearest and highly intense diffraction peaks which fit well with those of standard rutile TiO_2 (Powder Diffraction File No. 21-1276). This is important since rutile-phase TiO_2 is considered a very inefficient material in terms of its photocatalytic activity[1,2] and yet, we could obtain moderate photovoltaic activity by using the proposed structures here discussed.

3.2. Fourier-Transformed Infra-Red (FTIR) Spectrum of TiO_2:SiO_2 in Absorbance Mode

Similarly to the XRD measurements, all FTIR analyses were also performed for TiO_2:SiO_2 films deposited directly on glass slides (without metallization). The IR spectra for all samples are shown as absorption coefficient α after normalization of each sample to a single and averaged TiO_2 film thickness. Since these samples are quite different to a bulk and dense TiO_2 thin film, the TiO_2 nanoparticles tend to disperse within the SiO_2 matrix (generating empty spaces) thus avoiding normalization with respect to each physical thickness. All IR spectra were measured at between 1600 and 400 cm^{-1} of wavenumber and they were adjusted using the SOG-based oxide film as reference (SiO_2/Glass), in order to eliminate the influence of the highly absorbent peaks related to Si—O and Si—O—Si bonds;[15,16] especially those found at 1070 and 443 cm^{-1}, and which could screen-out the presence of any detectable Ti—O—Ti bonds; see Figure 3. The obtained IR spectra ~~includesome~~ absorption bands at 765 (black arrow at shoulder section), 530 and 395 cm^{-1}. The band detected as a shoulder at 765 cm^{-1} is comparable with the IR spectrum of crystalline TiO_2 (having anatase or rutile crystalline structure) due to symmetric stretching vibrations

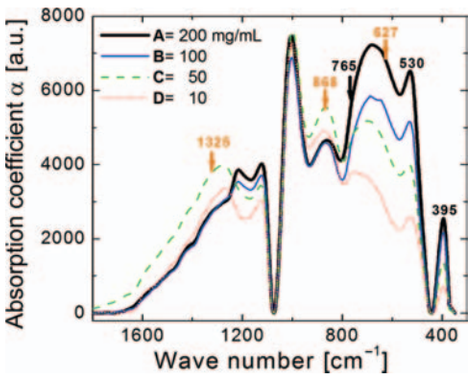

Fig. 3. Infra-Red spectra in absorbance mode, of films based on TiO_2 nanoparticles deposited directly on glass slides (all A–D samples) and using SiO_2/glass as reference.

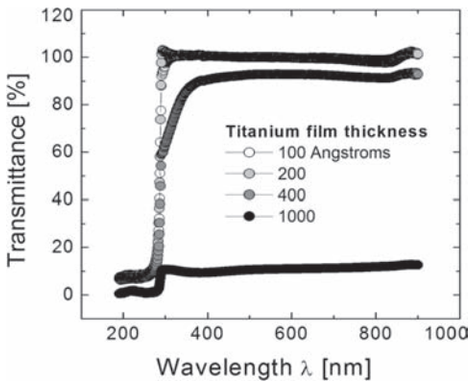

Fig. 4. ~~(Transmittance)~~ (UV-Vis) spectra of ultra-thin titanium films. The titanium film having 100 Å in thickness was used as the top electrode in the vertical Ti/TiO_2:SiO_2/Al/Glass MIM structures.

of the Ti—O bonds.[17] The absorption peaks for these Ti—O bonds increase with the content of TiO_2, confirming proper chemical bonding of this photocatalytic material for even the larger TiO_2 concentrations. Also, even though the main absorption bands for the Si—O—Si bonds mostly disappear when SOG-based oxide film is used as reference, some Si—O bonds appear in these samples surely because of vibrations of Si—O—Ti bonds, as observed in the band at 1005 cm^{-1}. On the other hand, the bands at 627 and 1325 cm^{-1} are thought to be related to vibrations of some Al—O bonds while the band at 868 cm^{-1} is related to a combination of both Al—O and Si—O bonding vibrations.[18] All these contributions make sense considering that commercial TiO_2 nanoparticles consist, according to the manufacturer, of 93% TiO_2, 2.5% Al_2O_3 and 3% SiO_2 (the remaining percentage consisting of other undetectable elements).

3.3. Band Gap Energy E_g of TiO_2 and Transmittance Spectra (UV-Vis) of Titanium Layers

Optical band gap is an important parameter in semiconductor materials because it allows knowing the threshold energies to which a material in particular, like TiO_2, is "transparent" or able to absorb incident photons and therefore, create electron–hole pairs that could participate in carrier transport processes in photoactive devices. After measuring and analyzing the UV-Vis spectra for the different concentrations of TiO_2nanoparticles (from 190 to 900 nm region), we noticed that transmittance is reduced in direct proportion to the TiO_2 concentration as expected.[14] Most importantly, ~~their~~extracted optical bandgap E_g is consistent and independent of film thickness (~~considering~~~~similar~~densities for all films) and is located at 3.11–3.12 eV. This calculated band gap energy E_g corresponds with the reported E_g for anatase or rutile TiO_2, between 3.0 and 3.2 eV respectively.[19–21]

On the other hand, for the vertical structure, we make use of an ultra-thin titanium stripe (see bottom-right inset of Fig. 1) in order to use it as a conductive top electrode while being able to transmit most of the UV-Vis irradiation through itself, thus allowing efficient photogeneration of carriers in the TiO_2. In order to obtain the optical properties of this electrode, the transmittance spectra (from 190 to 900 nm region) for different ultra-thin titanium films are shown in Figure 4. We clearly notice that the thinner titanium films (100 and 200 Å) transmit virtually the complete (100%) electromagnetic spectra from 900 nm down to 290 nm, thus being transparent to the visible, the UV-A and UV-B regions as well. For the UV-C region, all films readily absorb or reflect this energy so that the transmittance characteristics are lost. For a titanium film of 400 Å in thickness, the original transmittance falls to about 93% from 900 nm down to ~400 nm, thus this sample is transparent to only the visible region of the spectra. At wavelengths of 400 nm and downwards, this sample starts to absorb/reflect UV-A and UV-B thus it is not useful for proper absorption of those energies (by TiO_2) in the vertical structures. We also show the very low transmittance characteristics (around 10%) obtained from a thicker titanium film (1000 Å) as a reference.

3.4. Electrical Characterization Under Dark and Illumination Conditions (I–V-Light)

Before discussing the electrical characteristics of the horizontal (TiO_2:SiO_2/Al/Glass) and vertical (Ti/TiO_2:SiO_2/Al/Glass) photoactive structures, we measured the I–V characteristics under dark and UV illumination of only the titanium films (used as ultra-thin titanium electrodes on top of the active TiO_2:SiO_2 material) in order to confirm whether they produce any electrical response under illumination conditions or not. These measurements are important for the vertical photoactive structure since any change in the gate current I_g of that MIM stack is expected to come from photogeneration of carriers within the TiO_2 nanoparticles and no contribution is expected from the top titanium electrode. For this purpose, ultra-thin titanium stripes were evaporated on clean glass slides and their I–V-Light characteristics were measured. Figure 5 shows

ARTICLE

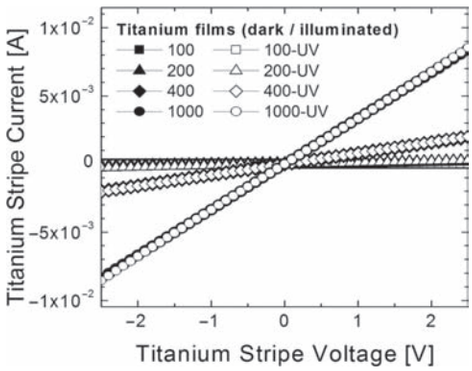

Fig. 5. *I–V*-Light characteristics of titanium stripeswith different physical thicknesses (only Ti/Glass stripes) before and after light irradiation. These electrodes did not present photovoltaic activity under UV irradiation.

the *I–V*-Light characteristics of titanium stripes (from 100 up to 1000 Å in thickness) under dark and UV conditions. We clearly see that there is no change whatsoever in the *I–V* slope of any of these films for both dark/UV conditions. Of course, the *I–V* slope only increases as the titanium films get thicker since it becomes more conductive (and less transparent at the same time). From the geometry of the titanium stripes and by taking into account every single thickness, the resistivity for all stripes was 1.9×10^3, 3.9×10^{-3}, 0.85×10^{-3} and 0.53×10^{-3} $\Omega \cdot$cm for the 100, 200, 400 and 1000 Å sample respectively. As expected, thicker titanium films get closer to the ideal resistivity value of bulk titanium, around 5×10^{-5} $\Omega \cdot$cm.[22]

Figure 6 shows the *I–V*-Light characteristics (under dark/illumination conditions) for the horizontal TiO_2:SiO_2/Al/Glass structures where, an *I–V* sweep was applied to the ends of the same aluminum stripe while limiting the current compliance to 100 mA. During the *I–V* sweep, dark, sunlight, sunlight + lamp and UV-B light (~300 nm) conditions were all applied on top of the structures so that the TiO_2 nanoparticles embedded within the SiO_2 layer (TiO_2:SiO_2 film) were the first material

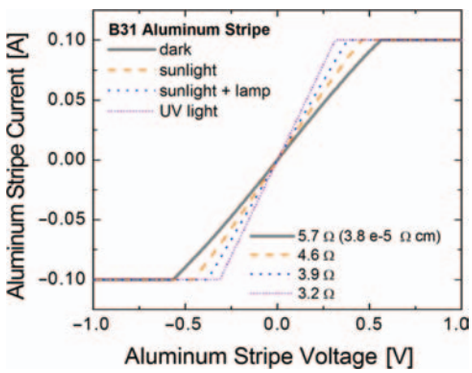

Fig. 6. *I–V*-Light characteristics of an aluminum stripe (horizontal TiO_2:SiO_2/Al/Glass structure) before and after light irradiation. This device acts as a *photoresistor*.

to absorb all possible irradiation coming from these light sources. Compared to dark conditions, photogeneration of excess carriers (both electrons and holes) within the TiO_2 nanoparticles is greater after UV-B light exposure and these carriers are directly transferred to both ends of the Al-stripe after applying a low potential difference. We notice a proportional change in the slope of the *I–V* measurement (change in the resistance) with respect to the energy of the light source used during irradiation. During UV-B light irradiation, the total aluminum resistance is reduced from 5.7 Ω down to 3.2 Ω (about 43%) which represent a moderate change in resistance given by a rather low quantum efficiency presented by this structure. Additionally, given that the maximum voltage observed during-proper *I–V*-Light modulation is around |0.25 to 0.5 V| and that the current compliance was set to 0.1 A, the maximum power delivered by this simple structure is then between 25 and 50 mW. On the other hand, given that some of the photogenerated carriers will be recombined or trapped within the SiO_2 matrix or at its interface with TiO_2 nanoparticles (any recombination/trapping mechanism), the "*horizontal path*" followed by photogenerated carriers during applied bias, is quite large (up to 18 mm) thus largely increasing their probability for recombination and trapping. In order to reduce the probability for carrier recombination and/or trapping phenomena, and thus, increase quantum efficiency during light irradiation, vertical structures were measured.

In the vertical structures, the top gate electrode is highly transparent to all UV-Vis irradiation so that when carriers are photogenerated, a vertical transition of these carriers between top/bottom electrodes (by an externally applied electric field) would require a shorter distance. For Ti/TiO_2:SiO_2/Al/Glass structure, the vertical transition of carriers before reaching the metal electrodes requires a distance of $d \leq 700$ nm, quite small compared to the length of a metal stripe (18 mm). This shorter distance d is then expected to reduce the probability for recombination and trapping of photogenerated carriers during

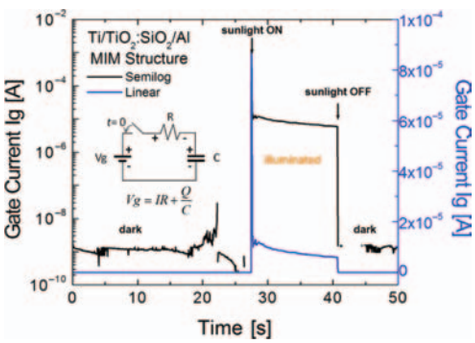

Fig. 7. *I–V*-Light characteristics of a MIM capacitor (vertical Ti/TiO_2:SiO_2/Al/Glass structure) before and after sunlight irradiation. The inset shows a very simplified electrical model of the vertical Ti/TiO_2:SiO_2/Al structure along with the basic capacitor charging equation. This device acts as a *photocapacitor*, thus enabling direct storage of solar energy after photogeneration of carriers.

applied bias. Figure 7 shows the I–V-Light characteristics (under dark/illumination conditions) for the vertical Ti/TiO_2:SiO_2/Al/Glass structures. The same data is shown in both linear and semilog formats for clarity purposes. Here, an I–V measurement in sampling mode (I-time) was used where the gate current I_g was constantly monitored with time and the gate voltage was kept constant ($V_g = 10$ V, applied at the semitransparent Ti electrode), all during dark and illumination conditions. In this case, and because of the lower gate current levels expected from a MIM capacitor like this, its gate current was limited to 100 μA. Also, we only used natural sunlight conditions (lower energy) during illumination. Interestingly, the gate current instantly increases from 10^{-9} up to 10^{-4} A (4 orders of magnitude) when this structure is exposed to sunlight conditions. We also notice the relatively high velocity response to optical excitation so that photogeneration of carriers is obtained more efficiently given the shortest vertical transition between electrodes. For this particular case, the positive and negative transitions between dark and illumination conditions results in transitions times of 26.78 and 87.2 ms respectively. Additionally, a slow decay time for the gate current I_g is observed when going from complete saturation of I_g to complete discharge of the device (from ON to OFF conditions). This latter characteristic is quite similar to that of a capacitor during the charging process because, in order to maintain a constant potential difference V_g (already applied to the capacitor), its charge Q increases while current I decreases. The inset shows a very simplified model of the vertical Ti/TiO_2:SiO_2/Al structure along with the basic capacitor charging equation. Finally, and in contrast with the *photoresistor* previously described, this MIM structure is quite similar in operation to that of a *photocapacitor*,[7,8] where all carriers could be efficiently stored within the capacitor itself right after photogeneration. In this sense, a light-driven self-charging capacitor having an efficient storage mechanism of solar energy could be obtained or in other words, enabling simultaneous conversion and storage of solar energy in the same device. This is highly important since these later devices have the potential to storage electric current during conversion of solar energy and then, use it anytime afterwards.

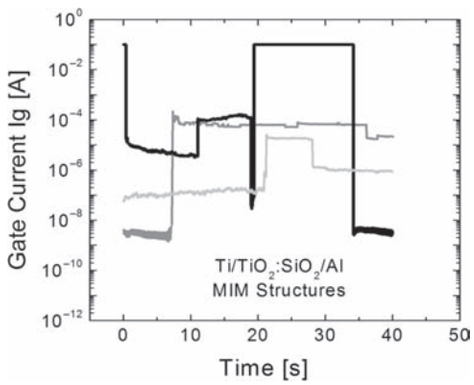

Fig. 8. I–V-Light characteristics of three different MIM capacitors (vertical Ti/TiO_2:SiO_2/Al/Glass structures) before and after sunlight irradiation. All samples present rapid dark-to-illuminated I_g transitions and vice versa.

Finally, Figure 8 shows the result of measuring three different Ti/TiO_2:SiO_2/Al vertical structures under dark and sun light conditions (the Y-axis is shown only in logarithmic format). Even though all samples present rapid dark-to-illuminated I_g transitions and vice versa, the gate current level I_g during illumination is quite disperse among all samples. These variations in I_g during sun light illumination could be originated from different physical, chemical and even, electronic mechanisms like trapping, recombination, phonon interaction, annihilation, interface defects, agglomeration of TiO_2 nanoparticles, ultra-thin titanium thickness variations, etc. Nonetheless, it is important to emphasize the huge change in the original resistance state of the TiO_2:SiO_2 material once it is illuminated with sun light (about 4 to 7 orders of magnitude), and this effect is what needs to be properly reproduced after optimizing the fabrication processing of these devices. Until now, we just demonstrate that TiO_2 nanoparticles can be used as photoactive material in devices having the ability to convert solar energy to an increased density of electronic current while keeping this current available in the form of a photocapacitor.

4. CONCLUSIONS

Photocarrier generation during light exposure (from sunlight up to UV-B irradiation conditions) of thin films based on rutile-phase TiO_2 nanoparticles has been observed. These TiO_2 nanoparticles are embedded within an inorganic SiO_2 matrix and used in *horizontal* TiO_2:SiO_2/Al/Glass and *vertical* Ti/TiO_2:SiO_2/Al/Glass structures. Both structures are fabricated using simple, economic and ultra-low thermal budget processing techniques, where the maximum processing temperature was 220 °C. For the horizontal structure, UV-B light exposure enables a reduction of the total resistance of an aluminum stripe by about 43%, thus acting as a very simple *photoresistor*. In vertical (MIM type) ~~structures,a~~ more efficient photogeneration of carriers is observed where this sample is illuminated under sunlight conditions. After illumination, the gate current I_g increases about 4 orders of magnitude (7 orders of magnitude for other samples) while this transition requires only 26.78 ms to occur. The vertical structure acts as a *photocapacitor* ~~because~~ it has the potential to enable direct storage of solar energy.

Acknowledgments: This work was fully supported by the National Council of Science and Technology (CONACYT-Mexico). Joel Molina thanks Dr. Miguel Angel Melendez (UDLAP) for his assistance in DLS measurements.

ARTICLE

References and Notes

1. Z. Ding, G. Q. Lu, and P. F. Greenfield, *J. Phys. Chem. B* 104, 4815 **(2000)**.
2. T. A. Kandiel, R. Dillert, A. Feldhoff, and D. Bahnemann, *J. Phys. Chem.* 114, 4909 **(2010)**.
3. M. A. Behnajady, N. Modirshahla, M. Shokri, and B. Rad, *Global NEST Journal* 10, 1 **(2008)**.
4. D. H. Kim, D. K. Choi, S. J. Kim, and K. S. Lee, *Catalysis Communications* 9, 654 **(2008)**.
5. C. D. Valentin, G. Pacchioni, and A. Selloni, *Phys. ReV. B* 70, 085116 **(2004)**.
6. O. Diwald, L. Thompson, E. G. Goralski, S. D. Walck, and J. T. Yates, *J. Phys. Chem. B* 108, 52 **(2004)**.
7. T. Miyasaka and T. N. Murakami, *Appl. Phys. Lett.* 85, 3932 **(2004)**.
8. C. W. Lo, C. Li, and H. Jiang, *Proceedings of the 2010 International Conference on Optical MEMS and Nanophotonics*, Sapporo, Japan, August **(2010)**, p. 65.
9. T. Song and B. Sun, *ChemSusChem.* 6, 408 **(2013)**.
10. X. Zhang, X. Huang, C. Li, and H. Jiang, *Adv. Mater.* ~~1~~ **(2013)**.
11. W. Guo, X. Xue, S. Wang, C. Lin, and Z. L. Wang, *Nano Lett.* 12, 2520 **(2012)**.
12. M. S. Nuckowska, K. Grzejszczyk, P. J. Kulesza, L. Yang, N. Vlachopoulos, L. Häggman, E. Johansson, and A. Hagfeldt, *J. of Power Sources* 234, 91 **(2013)**.
13. J. Tauc, *MRS Bulletin* 3, 37 **(1968)**.
14. J. Molina, C. Zuniga, E. Gutierrez, E. Mendoza, J. L. Sanchez, and E. R. Bandala, *Proceedings of The Fourth International Conference on Sensor Device Technologies and Applications* (*SENSOR DEVICES 2013*), Barcelona, Spain, August **(2013)**, ~~Vol. 41~~,
15. S. Music, N. F. Vincekovic, and L. Sekovanic, *Braz. J. Chem. Eng.* 28, 89 **(2011)**.
16. T. Lopez, E. Sanchez, P. Bosch, Y. Meas, and R. Gomez, *Mater. Chem. Phys.* 32, 141 **(1992)**.
17. A. N. Murashkevich, A. S. Lavistkaya, T. I. Barannikova, and I. M. Zharskii, *J. Appl. Spectrosc.* 75, 730 **(2008)**.
18. D. N. Goldstein, J. A. McCormick, and S. M. George, *J. Phys. Chem. C* 112, 19530 **(2008)**.
19. J. Dharma and A. Pisal, *App Note, Perkin-Elmer Inc.* ~~1~~ **(2009)**.
20. S. Valencia, J. M. Marin, and G. Restrepo, *Open Mater Sci. J.* 5404, 9 **(2010)**.
21. D. R. Coronado, G. R. Gattorno, M. E. Pesqueira. C. Cab, R. Coss, and G. Oskam, *Nanotechnology* 19, 145605 **(2008)**.
22. B. Singh and N. A. Surplice, *Thin Solid Films* 10, 243 **(1972)**.